192-Channel CMOS Neurochemical Microarray

Meisam Honarvar Nazari[1], Hamed Mazhab-Jafari[1], Lian Leng[2], Axel Guenther[2] and Roman Genov[2]

[1]Department of Electrical and Computer Engineering and [2]Department of Mechanical and Industrial Engineering
University of Toronto, Toronto, ON M5S 3G4, Canada
Email: roman@eecg.utoronto.ca

***Abstract*— A 16×12-channel neurochemical microarray is presented. Each channel acquires bidirectional currents down to pico-amperes proportional to the concentration of a neurochemical. By combining the current-to-frequency and the single-slope analog-to-digital converter (ADC) 110dB of dynamic range is achieved. The ADC in each channel generates a 16-bit output in less than a millisecond. The microarray with flat and 3D gold electrodes and an on-chip microfluidic network is experimentally validated in in-situ recording of neurotransmitter dopamine.**

I. Introduction

Potentiostatic amperometric integrated circuits [1,2,3] are gaining popularity in biochemical sensory applications such as monitoring of chemical neural activity of the brain [4,5,6,7] and DNA detection [8,9,10]. In brain neurochemistry, dysfunctions of neurotransmitters such as dopamine, glutamine and serotonine have been linked to neural disorders such as stroke, Parkinson's and Alzheimer's diseases.

Concentrations of neurochemicals can be measured by a potentiostat circuit. As shown in Fig. 1, a potentiostat measures the current through the working electrode (WE) held at a fixed potential. The reference electrode (RE) is set to a constant voltage for constant-potential amperometry (CA), a bidirectional ramp voltage for cyclic voltammetry (CV), or a small-amplitude sinusoid for impedance spectroscopy (IS). The recorded current value or its waveform features indicate the level of biomolecular reactions due to reduction and oxidation (redox) or charge fluctuations at the electrode surface. Low concentrations of neurochemicals result in pA-level input currents that have to be sampled at the ksps-range sampling rate.

We present a 192-channel integrated potentiostat array depicted in Fig. 2 that implements all three sensory methods to simultaneously measure concentration of multiple neurochemicals, as many as one per channel, directly on the chip. The 3.8×3.1 mm^2 array implemented in a 0.35μm CMOS technology consists of two 8x12 sub-arrays, one for single-ended (upper) and one for differential (lower) amperometry. For simplicity only the single-ended configuration is described in this paper. The current-to-frequency ADC and the single-slope ADC architectures are combined and reuse the same circuits to yield high sensitivity at ksps sampling rate. Biocompatible on-chip gold microelectrodes yield high sensitivity and selectivity, eliminate costly excessive wiring and minimize the interference noise. A low cost on-chip microfluidic network integrated with the CMOS potentiostat array allows for per-channel sample delivery, provides for faster analysis and response times and a better overall process control.

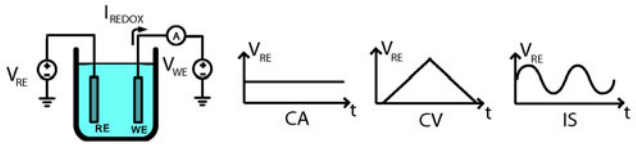

Fig. 1. Potentiostat principle of operation in three sensory methods: constant potential amperometry (CA), cyclic voltammetry (CV) and impedance spectroscopy (IS).

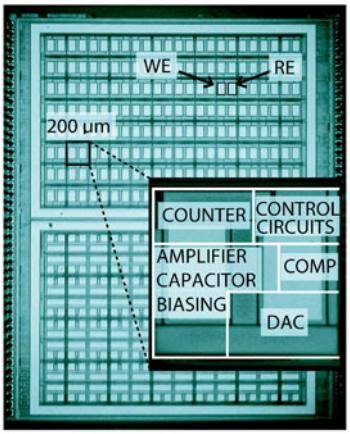

Fig. 2. Die micrograph of the 192-channel integrated potentiostat. The die size is 3.8×3.1 mm^2 in a 0.35μm CMOS technology.

II. VLSI Implementation

Each channel is comprised of a low-noise current conveyer followed by an analog-to-digital converter (ADC) as shown in Fig. 3. The current conveyer at the front end of each channel maintains the working electrode potential, V_{WE}, as needed to induce a redox reaction. It employs a folded-cascode amplifier to provide a wide-swing output. To achieve both a wide dynamic range and a short conversion time, the ADC architecture combines two analog-to-digital conversion techniques, the current-to-frequency ADC and the single-slope ADC as described by the timing diagrams in Fig. 3.

The current-to-frequency ADC generates the MSBs in the first, coarse conversion phase. In the second, fine conversion phase, the LSBs are extracted by the single-slope ADC. Both

978-1-4244-5760-1/10/$26.00 ©2010 IEEE

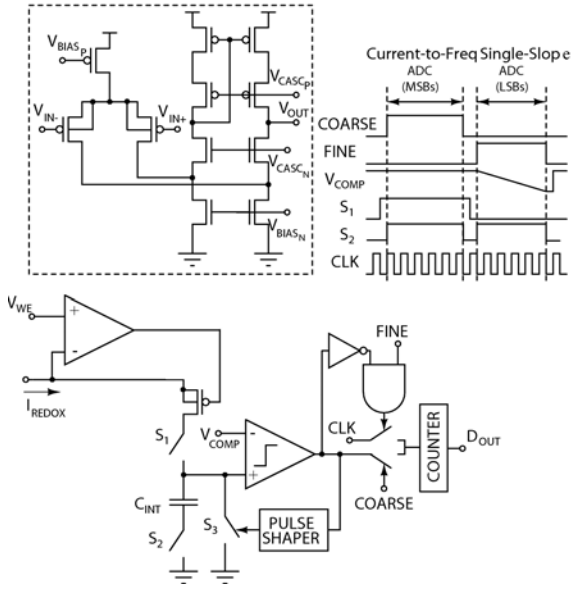

Fig. 3. Top-level architecture of one channel of the integrated potentiostat and the timing diagram of the ADC.

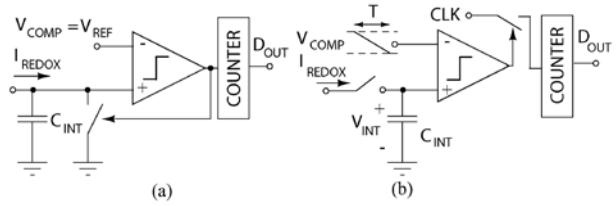

Fig. 4. The ADC architecture: (a) the current-to-frequency analog-to-digital conversion phase, and (b) the single-slope analog-to-digital conversion phase.

ADCs reuse most of the same circuit components. As shown in Fig. 4(a), during the coarse conversion phase, the current continuously charges the integrating capacitor. The comparator generates a reset pulse when the voltage across the capacitor reaches V_{REF} to discharge the integrating capacitor. A pulse shaping circuit widens the pulse so that it fully discharges the capacitor. The number of the ADC output pulses is directly proportional to the input current. A counter counts the number of pulses generated during this phase and produces the MSBs. A wide input dynamic range is achieved as data conversion is performed in the time domain. This comes at a cost of a longer conversion time, as for a low input current a long time is needed to charge the integrating capacitor. To eliminate this trade-off, the single-slope ADC architecture is employed in the second phase of the data conversion. The output of the first phase is related to the input current as

$$I_{IN} = \frac{N_{MSB}\ C_{INT}\ V_{REF}}{T_{phase1}} + \Delta I, \qquad (1)$$

where I_{IN} is the input redox current, T_{phase1} is the duration of phase one, N_{MSB} is the number of output pulses, C_{INT} is the integrating capacitance, V_{REF} is the comparator reference

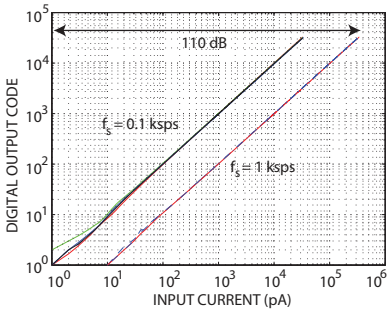

Fig. 5. Experimentally measured transfer characteristics of four adjacent channels in one column of the potentiostat array for two sampling frequency.

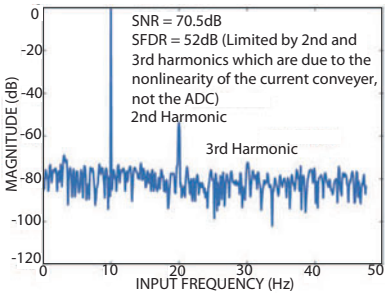

Fig. 6. Experimentally measured output spectrum of the ADC for a 10Hz sinusoidal input.

voltage during the first phase , and ΔI is the residue current which is resolved in the second phase.

Upon completion of the first phase, the remaining voltage across the integrating capacitor is held as an input to the single-slope ADC to extract the LSBs, as shown in Fig. 4(b). The comparator reference voltage generated by an in-channel DAC starts ramping down and the input of the counter is switched to a periodic clock signal. The counter counts the number of clock cycles that the ramp reference voltage requires to reach the capacitor voltage. To eliminate input-dependent charge injection switch S_2 in Fig. 3 turns off slightly before S_1 turns off, leaving no path through C_{INT} for the channel charge of S_1 to flow and introduce an input-dependent error. The output after the two phases is related to the input current as

$$I_{IN} = \frac{C_{INT}\ V_{REF}}{T_{phase1}} \left[N_{MSB} + \frac{N_{LSB}}{2^M} \right], \qquad (2)$$

where N_{LSB} is the output of the counter in the second phase and M is the number of bits extracted in the second phase.

The digital outputs of four channels with the input current swept between 1pA and 350nA are shown in Fig. 5. The input dynamic range is 110dB cumulatively for the two sampling frequency settings, or 90.9dB at 1ksps sampling rate. Dynamic performance of an entire channel was measured by applying a sinusoidal input current. Fig. 6 shows the power spectral density of the quantized output. The output SNDR is limited by the non-linearity of the current conveyer, not the ADC. The resulting effective number of bits (ENOB) is

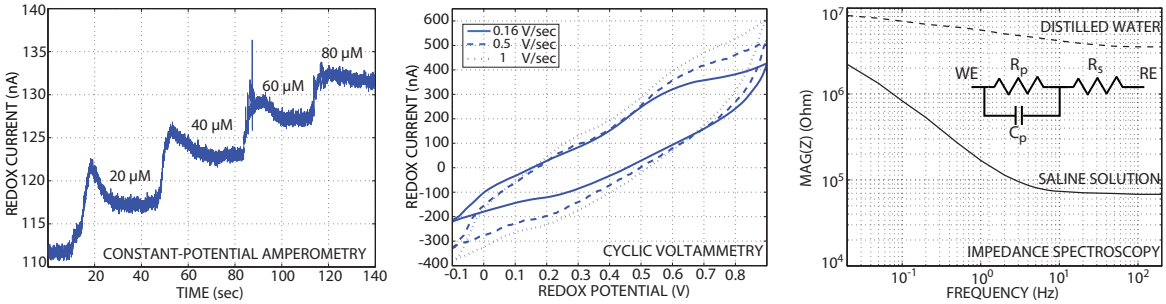

Fig. 7. Experimentally measured results of (a) dopamine constant-potential amperometry, (b) buffer cyclic voltammetry, and (c) impedance spectroscopy.

TABLE I
EXPERIMENTALLY MEASURED CHARACTERISTICS

Technology	0.35μm CMOS
Supply Voltage	3.3V
Die Area	3.8mm×3.1mm
Array Dimensions	16×12 channels
Channel Size	200μm×200μm
Sampling Rate	1ksps
ADC Resolution	16-bit
Sensitivity	1pA
Channel SNR (fs=1ksps)	11.32 bits
Channel SFDR (fs=1ksps)	8.3 bits
Channel Power Consumption	
Current conveyer	80μW
Comparator	63μW
Biasing	23μW
Digital	22μW
Total	188μW

11.3. Table I provides a summary of experimentally measured characteristics of the integrated potentiostat.

III. EXPERIMENTAL RESULTS

The utility of the microarray in neurochemical sensing was validated by experimentally measuring the concentration of neurotransmitter dopamine and a buffer. Results of constant-potential amperometry of dopamine in 0.1 mM phosphate buffered saline solution with off-chip working and reference electrodes at 300mV redox potential are shown in Fig. 7(a). The steps in the recorded current accurately correspond to the addition of controlled amounts of dopamine. Cyclic voltammetry recording results depicted in Fig. 7(b) demonstrate recording of redox currents at the maximum 1ksps sampling rate. A 0.01M phosphate buffered saline solution was measured at three different scan rates yielding progressively tilted voltammograms. In order to avoid a large background current, low sweep rates were utilized. An impedance spectroscopy experiment was performed by applying a small-amplitude sinusoidal potential to an off-chip reference electrode placed first in distilled water and then phosphate buffered saline solution. The correct frequency domain representation of the impedance between electrodes was generated by sweeping the frequency of the sinusoidal potential as shown in Fig. 7(c).

Both 2D and 3D biocompatible microelectrodes have been fabricated on the surface of the potentiostat die for on-chip spatial biochemical sensing. An array of 192 gold plate microelectrodes was electrolessly plated with a 2μm-thick Ni base and 0.75μm-thick gold as shown in Fig. 8 (top, left). The 3D microelectrodes are 100μm-long gold bumps [11] bonded to the die as depicted in Fig. 8 (top, right). The large surface area of these 3D microelectrodes increases their sensitivity. They can also be used for neurochemical activity monitoring in acute brain slices in in-vitro animal studies, as the pointed shape allows for penetrating a thin ($\sim$50μm) layer of dead tissue caused by tissue slicing. After the electrode fabrication, the die is wire-bonded and the bonding wires are insulated with a biocompatible epoxy as depicted in Fig. 8 (bottom, left). In order to demonstrate the on-chip spatial recording functionality of the potentiostat, dopamine constant-potential amperometry was performed on the array of on-chip 3D gold electrodes. A drop of dopamine in the phosphate buffered saline solution was placed in the corner of electrode array. Fig. 8 (bottom, right) depicts the two recorded (thresholded) images capturing the front of the flow of dopamine on the surface of the chip.

For rapid biochemical sensing on a low-cost miniature platform, the potentiostat die was integrated with a two-layer PDMS microfluidic chamber as depicted in Fig. 9 (top, left). An example of the bottom layer fluidic chamber is shown in Fig. 9 (top, right). Fig. 9 (bottom, left) depicts a micrograph of the fluidic chamber in Fig. 9 (top, right) compression-sealed against the surface of the potentiostat die. Fig. 9 (bottom, right) shows the impedance spectroscopy results (thresholded) measured by the potentiostat when dopamine was flowing through the chamber over one sub-array on the die.

Table II provides a comparative analysis of the presented design and existing amperometric biochemical sensory microsystems.

IV. CONCLUSIONS

The microarray enables simultaneous analysis of up to 192 neurochemicals in parallel. The 200μm-pitch channel count

TABLE II

COMPARATIVE ANALYSIS OF REPORTED AMPEROMETRIC SENSORY MICROSYSTEMS

	Tech (μm)	Channel Count	Conversion Rate (Hz)	Channel Power (μW)	Channel Area (mm^2)	Dynamic Range	Sensitivity (pA)	On-chip Electrodes 2D/3D	On-chip Microfluidics	Sensory Methods CA/CV/IS
ISSCC 94 [1]	2	1	330	5000	4.84	100fA-40mA	0.1	-/-	-	-/Yes/-
JSSC 04 [9]	0.5	128	10	N/A	0.1	1pA-100nA	1	Yes/-	-	Yes/-/-
TCAS-I 06 [3]	0.5	42	3	11.5	0.086	-/+100nA	0.05	-/-	-	Yes/-/-
TCAS-I 06 [7]	0.5	1	3	5500	0.7	3pA-10uA	1	-/-	-	-/Yes/-
ISSCC 08 [8]	0.6	24	10	N/A	N/A	-/+100nA	100	Yes/-	-	-/Yes/-
JSSC 08 [2]	0.25	16	2500	N/A	0.12	100pA-250nA	100	Yes/-	-	-/Yes/-
JSSC 09 [5]	0.5	4	5000	76	N/A	-/+750nA	8	-/-	-	-/Yes/-
ISSCC 10 [10]	0.35	100	10	848	0.01	330-41μA	330	Yes/-	-	-/-/Yes
This Work	**0.35**	**192**	**1000**	**188**	**0.04**	**1pA-350nA**	**1**	**Yes/Yes**	**Yes**	**Yes/Yes/Yes**

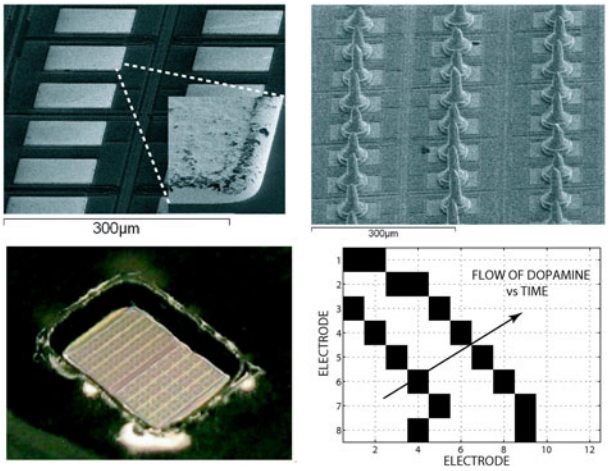

Fig. 8. On-chip 2D (top, left) and 3D (top, right) gold electrodes, encapsulated die (bottom, left) and experimental results of constant potential amperometry recording of a dopamine solution flow front (bottom, right).

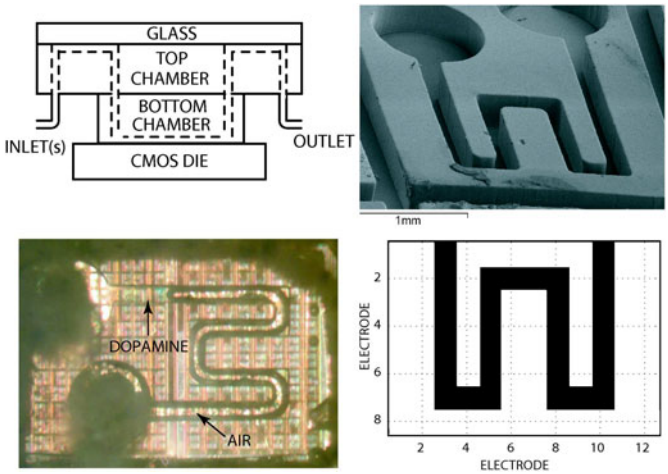

Fig. 9. Cross-sectional view of the on-chip two-layer PDMS microfluidic chamber (top, left), microfluidic network (top, right), fluidic chamber compression-sealed against the surface of the potentiostat die (bottom left), and experimentally measured results of on-chip impedance spectroscopy of dopamine (bottom, right).

scales proportionally with the area as needed for rapid large-scale monitoring and diagnostics of various neural disorders related to neurochemical dysfunction. On-chip 3D gold electrodes are a promising sensor modality for future tissue-penetrating and implantable brain neurochemistry analysis applications.

REFERENCES

[1] R.J. Reay, S.P. Kounaves, and G.T.A. Kovacs, "An integrated CMOS potentiostat for miniaturized electroanalytical instrumentation," *IEEE Int. Solid-State Circuits Conf. (ISSCC)*, pp. 162-163, 1994.

[2] P.M. Levine, P. Gong, R. Levicky, K.L. Shepard, "Active CMOS Sensor Array for Electrochemical Biomolecular Detection," *IEEE J. Solid-State Circuits,* pp. 1859-1871, August 2008.

[3] A. Gore, S. Chakrabartty, S. Pal, and E. C. Alocilja, "A multichannel femtoampere-sensitivity potentiostat array for biosensing applications," *IEEE Trans. Circuits and Systems II*, vol. 53, no. 11, pp. 2357-2363, Nov. 2006.

[4] R. Genov, M. Stanacevic, M. Naware, G. Cauwenberghs, and N. Thakor, "16-Channel integrated potentiostat for distributed neurochemical sensing," *IEEE Trans. Circuits and Systems I*, Vol. 53, No. 11, pp. 2371-2376, Nov. 2006.

[5] M. Roham, M.P. Garris, and P. Mohseni, "A Wireless IC for Time-Share Chemical and Electrical Neural Recording," *IEEE J. Solid-State Circuits,* pp. 3645 - 3658 , 2009.

[6] M. Stanacevic, K. Murari, G. Cauwenberghs, and N. Thakor, "VLSI potentiostat array with oversampling gain modulation for wide-range neurotransmitter sensing," *IEEE Trans. Bio Circuits and Systems*, vol. 1 (1), pp. 63-72, 2007.

[7] F. Laiwalla, K. G. Klemic, F. J. Sigworth, and E. Culurciello, "An integrated patch-clamp amplifier in silicon-on-saphire CMOS," *IEEE Trans. Circuits and Systems I*, vol. 53, no. 11, pp. 2364-2370, Nov. 2006.

[8] F. Heer, M. Keller, G. Yu, J Janata, M Josowicz, A Hierlemann, "CMOS Electro-Chemical DNA-Detection Array with On-Chip ADC," *IEEE Int. Solid-State Circuits Conf. (ISSCC)*, pp. 168-169, 2008.

[9] M. Schienle, C. Paulus, A. Frey, F. Hofmann, B. Holzapfl, P. Schindler-Bauer, and R. Thewes, "A fully electronic DNA sensor with 128 positions and in-pixel A/D conversion," *IEEE J. Solid-State Circuits,* vol. 39, no.12, pp. 2438-2445, 2004.

[10] Arun Manickam, Aaron Chevalier, Mark McDermortt, A.D. Ellington, A. Hassibi, "A CMOS Electrochemical Impedance Spectroscopy Biosensor Array for Label-Free Biomolecular Detection", *IEEE Int. Solid-State Circuits Conf. (ISSCC)*, pp. 130-131, 2010.

[11] J. Aziz, R. Genov, M. Derchansky, B. Bardakjian, P. Carlen, "256-Channel Neural Recording Microsystem with On-Chip 3D Electrodes," *IEEE Int. Solid-State Circuits Conf. (ISSCC)*, pp. 160-161, 2007.